ACI STRUCTURAL JOURNAL TECHNICAL PAPER

Title No. 114-S102

Effect of Openings on Punching Shear Strength of Reinforced Concrete Slabs—Finite Element Investigation

by Aikaterini S. Genikomsou and Maria Anna Polak

Finite element formulation with the damaged plasticity model for concrete in ABAQUS is used to simulate the opening effect in reinforced concrete slabs without shear reinforcement. Nine edge slab-column connections, previously tested, are analyzed. The effect of the location and the size of the opening on the punching shear resistance is investigated. The numerical results from the finite element analyses (FEA) are in good agreement with the experimental results in terms of ultimate load and cracking; and confirm the accuracy of the proposed finite element model. The punching shear capacity of the tested specimens is calculated using the equations of ACI 318-14 and compared with the test and numerical results. Then, parametric investigation is presented on edge and interior specimens having openings with different sizes and located in different distances from the column. The results confirm that the punching shear resistance is decreased with an increase in opening size and with the decrease in opening distance from the column.

Keywords: damaged plasticity model; design code; finite element analysis; opening effect; punching shear.

INTRODUCTION

Punching shear failure can happen in reinforced concrete flat slabs due to the development of high shear stresses in the slab-column connection area. These shear stresses become higher when openings and unbalanced moments exist. Openings reduce the area of concrete sustaining shear stresses. Unbalanced moments that are present due to the geometry of a slab, loading conditions, and the presence of openings increase the applied shear stresses. The openings are created for reasons such as ventilation, air-conditioning, heating, and electrical reasons; and due to architectural reasons these openings are usually created next to columns, leading to a reduction of the volume of concrete that can resist punching shear.

Although concrete flat slabs started to be extensively tested in the 1950s by Elstner and Hognestad (1956) and later by Moe (1961), the phenomenon of openings in these slabs was first examined only on interior slab-column connections (Moe 1961; Hognestad et al. 1964; Mowrer and Vanderbilt 1967; Roll et al. 1971). In the following years, no research was reported in slabs having openings. Again, in the 1990s, the effect of opening in reinforced concrete slabs started to be examined by recent researchers, such as El-Salakawy et al. (1999), Teng et al. (2004), Bu and Polak (2009), Borges et al. (2013), Anil et al. (2014), and Ha et al. (2015). El-Salakawy et al. (1999) tested edge slabs with one opening of a different size and location from the column. The test results showed the effect of the opening in the reduction of the punching shear strength of the slabs. Teng et al. (2004) and Borges et al. (2013) examined the effect of openings in reinforced concrete slabs and proposed methods to consider the critical perimeter.

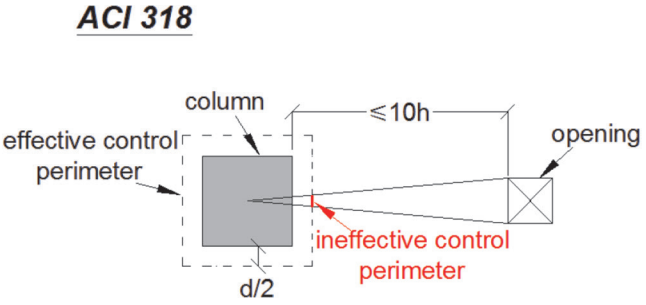

Fig. 1—Critical perimeter near opening according to ACI 318-14.

The research work done by Moe (1961) was the basis to be considered the effect of openings in slabs by Joint ACI-ASCE Committee 326 (1962). Moe (1961) tested 15 slabs with different patterns of openings adjacent to the column. The tests showed that the ultimate shear strength of the slabs depends on the size and location of the openings with respect to the loaded area (column) and the thickness of the slab. Joint ACI-ASCE Committee 326 (1962) considered the effect of the openings on the shear strength of the slabs by reducing the critical perimeter, which was assumed to be at a distance of $d/2$ from the loaded area. The reduction of the critical perimeter was considered with a similar way, as it is considered in the current ACI 318-14 code (ACI Committee 318 2014). ACI 318-14 adopts the critical shear perimeter at a distance $d/2$ from the loaded area (column), where d denotes the effective depth of the slab. A reduction of the critical perimeter depending on the size and the location of the opening is considered, which is a part of the perimeter contained between two tangents drawn to the outline of the opening from the center of the loaded area (top surface of column) is considered to be ineffective. ACI 318-14 considers the reduction in the critical perimeter if the shortest distance between the perimeter of the loaded area (column) and the edge of the opening is smaller or equal to $10h$, where h is the thickness of the slab (refer to Fig. 1).

Nonlinear finite element analysis (FEA) can be viewed as a method to examine the structural behavior and to supplement the existing experimental database of concrete flat

ACI Structural Journal, V. 114, No. 5, September-October 2017.
MS No. S-2016-359.R1, doi: 10.14359/51689871, was received October 27, 2016, and reviewed under Institute publication policies.

slabs having openings. The condition for this approach to be reliable is to have the FEA procedure calibrated on test results (Genikomsou and Polak 2015). In literature, to the best knowledge of the authors, only Guan and Polak (2007) used a nonlinear layered two-dimensional finite element method to examine the opening effect in edge concrete slabs. In the study presented herein, three-dimensional (3-D) FEA is conducted to analyze reinforced concrete slab-column connections with openings previously tested by El-Salakawy et al. (1999). The analyses are performed using the FEA software ABAQUS (2010) with the coupled damaged-plasticity model for concrete. The concrete damaged plasticity model in ABAQUS is employed with the fictitious crack model introduced by Hillerborg (1985).

In this paper, a brief description of the constitutive concrete damaged plasticity model used in ABAQUS is presented first. Then, the FEA results are presented for the slab-column connections. The numerical results are compared to the test results in terms of ultimate load, ultimate displacement, and crack propagation, showing the predictive capability of the calibrated finite element model in analyzing concrete flat slabs with openings. The parametric investigation regarding the effect of the distance of the opening from the column and the size of the openings is presented. The parametric studies consider both edge and interior slab-column connections. Twelve edge slab-column connections and 30 interior slab-column connections with varying location and size of the openings are analyzed. Finally, ACI 318-14 provisions for punching shear capacity of slabs with openings are discussed.

RESEARCH SIGNIFICANCE

Openings in concrete flat concrete slabs have to be created for many reasons; among others, to accommodate utility ducts in buildings. These openings are usually constructed next to columns; therefore, they reduce the punching shear capacity of the slabs. The existing experimental database of reinforced concrete flat slabs with openings is limited; thus, the effect of the openings on the punching shear strength of the slabs needs to be investigated. Properly calibrated FEA can be used as a tool for extending information on the effect of openings in slabs. In this work, the results from the finite element simulations of existing slabs with openings are presented and compared to the test results. Comparing the behavior of slabs with different size and location of openings, significant conclusions can be offered regarding the punching shear resistance and cracking propagation. The already-calibrated concrete damaged plasticity model in ABAQUS (2010) is employed for this study (Genikomsou and Polak 2015). Comparison between the predictions from ACI 318-14, test, and numerical results regarding the punching shear capacity of the slabs with openings is shown. The parametric investigation considers edge and interior slabs with openings of different sizes and located at different distances from the column with the aim to show the need for possible future code modifications for ACI 318-14 regarding the way that the effect of openings is considered into the design equations. The paper investigates the ACI 318-14 provisions regarding the distance of the opening from the column at which the effect of the opening diminishes.

SUMMARY OF EXPERIMENTAL WORK

Nine edge slab-column connections (XXX, SF0, SE0, SF1, SF2, CF0, HXXX, HSF0, and HSE0) are analyzed. These slabs were previously tested under a vertical shear force (P) applied on the top of the upper column and two lateral forces (F) applied at column ends in three stages (El-Salakawy et al. 1999). In the first stage, the loads were increased with a loading rate of 2.5 kN/min (0.6 kip/min) until reaching the service load of $P = 43$ kN (9.7 kip). Then the load was cycled 10 times between the dead and the dead plus the live loads to simulate the fluctuations of the live loads. At the final stage, the load was increased at 1.5 kN/min (0.34 kip/min) loading rate until each specimen failed. The ratio between the unbalanced moment (M) produced by the two horizontal forces (F) and the vertical shear force (P) was equal to 0.3 m (11.81 in.) for Specimens XXX, SF0, SE0, SF1, SF2, CF0, and 0.66 m (25.98 in.) for Specimens HXXX, HSF0, and HSE0 to account for the additional moment, which may affect the slab-column connection due to the horizontal loads. These ratios were kept constant during the whole loading process. All specimens had the same dimensions (1540 x 1020 x 120 mm [60.63 x 40.16 x 4.72 in.]) with the top and bottom column stubs (250 x 250 mm [9.84 x 9.84 in.]) extending out 700 mm (27.56 in.). The column was reinforced with six 25M bars and with 8M@115 mm (4.53 in.) ties. The yield strength of the reinforcing steel in column is equal to 340 MPa (49.31 ksi). The effective depth of all slabs was 90 mm (3.54 in.) with 20 mm (0.79 in.) clear cover of concrete. The horizontal loads were applied at distance 600 mm (23.62 in.) from the top and bottom faces of the slabs. The size of the openings was 150 x 150 mm (5.91 x 5.91 in.) for all slabs, except for Slab CF0, which had an opening 250 x 250 mm (9.84 x 9.84 in.)—same size with the column. Additional reinforcement was placed around the openings equivalent to that interrupted by the openings. The average tension reinforcement ratio of the slabs in both directions was equal to 0.75% and the compression reinforcement ratio in both directions was 0.45%. The loading process, dimensions of the specimens, and location of the openings are presented in Fig. 2. The compressive strength of concrete of all slabs together with the experimental results are presented in Table 1. Table 2 shows the material properties of the flexural reinforcement.

FINITE ELEMENT SIMULATIONS

Dye to symmetry, one half of the slab-column connections was simulated in ABAQUS (2010). The symmetry was not considered for Specimens SE0 and HSE0; thus, the whole slabs were analyzed. Six square elements of 20 mm (0.79 in.) were meshed through the depth of the slabs. Concrete was modeled with eight-noded hexahedral with reduced integration elements (C3D8R) and the reinforcement was modeled using 3-D two-noded truss elements (T3D2) that can transmit only axial loads. In ABAQUS (2010), the C3D8R finite elements are continuum stress/displacement three-dimensional (3-D) first-order solid elements with

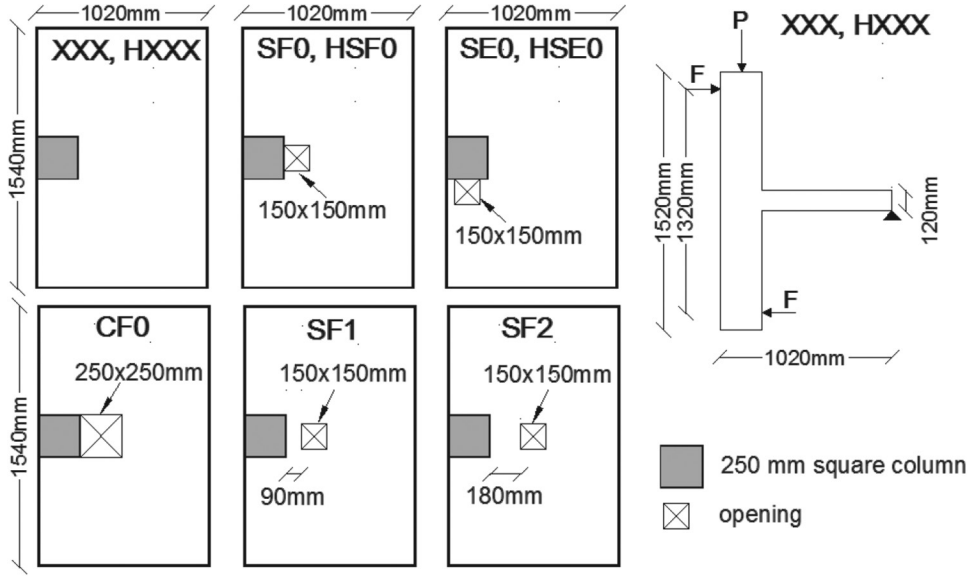

Fig. 2—Schematic drawings of specimens with their dimensions. (Note: 1 mm = 0.0394 in.).

Table 1—Material properties of concrete and test results

Slab	f_c', MPa (ksi)	M/P, m (in.)	Failure load, kN (kip)	Failure displacement, mm (in.)
XXX	33 (4.786)	0.3 (11.81)	125 (28.10)	15.06 (0.593)
SF0	31.5 (4.569)	0.3 (11.81)	110 (24.73)	15.95 (0.628)
SE0	32.5 (4.714)	0.3 (11.81)	120 (26.98)	15.55 (0.612)
SF1	33 (4.786)	0.3 (11.81)	115 (25.85)	15.02 (0.591)
SF2	30 (4.351)	0.3 (11.81)	114 (25.63)	13.44 (0.529)
CF0	30.5 (4.424)	0.3 (11.81)	86 (19.33)	11.01 (0.433)
HXXX	36.5 (5.294)	0.66 (25.98)	69 (15.51)	5.96 (0.235)
HSF0	36 (5.221)	0.66 (25.98)	58 (13.04)	6.95 (0.274)
HSE0	36.5 (5.294)	0.66 (25.98)	65 (14.61)	5.26 (0.207)

Table 2—Material properties of flexural reinforcement

Steel layer	Bar size	f_y, MPa (ksi)	ε_y	f_t, MPa (ksi)	ε_t	E_s, MPa (ksi)
Compressive	5M	430 (62.37)	0.0022	600 (87.02)	0.15	195,000 (28,282,358.9)
Tensile	10M	545 (79.05)	0.0027	900 (130.53)	0.10	180,000 (26,106,792.8)

reduced integration. Reduced integration was chosen for these elements to avoid the shear-locking problem. Perfect bond between concrete and reinforcement was considered through the embedded method. However, the interaction between concrete and reinforcement is indirectly considered through the concrete material modeling by using tension stiffening for the tensile behavior as it is described in the following section. Simple supports were introduced at the bottom along the edges of the slabs. Quasi-static analysis in ABAQUS (2010) /Explicit solver was performed for all specimens. Even if the explicit methods demand a large number of increments, the equations are not solved in each increment, and with this way a smaller computational cost per increment compared to an implicit method is required, making the ABAQUS (2010) /Explicit solver well-suited for nonlinear problems. For accuracy in quasi-static analyses, a smooth amplitude curve should be adopted simulating the increasing displacement or velocity. In these numerical analyses, the vertical load was started to be applied through the column stub with an increasing rate and then it was kept constant. The horizontal loads applied to the top and bottom columns were simulated using a displacement-controlled analysis because, during the tests, the horizontal loads were increased until the specimens failed. Mass scaling was not considered for reducing the computational solution time in the analyses and the energy balance equation was evaluated at the end of each analysis to estimate whether each simulation has produced a proper quasi-static response. The concrete damaged plasticity model offered in ABAQUS (2010) was chosen for the analyses. It should be noted that the material modeling parameters, the finite element mesh, and the boundary conditions were previously calibrated and validated based on an extensive study of an interior slab-column connection (SB1), which was described in detail in the work done by Genikomsou and Polak (2015).

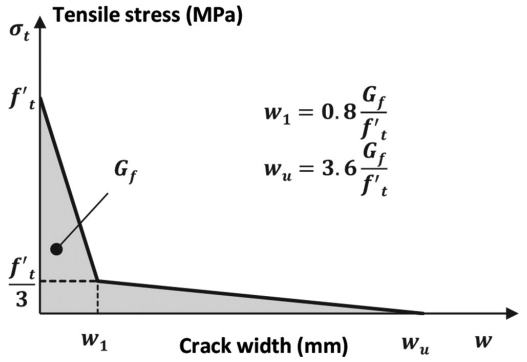

Fig. 3—Uniaxial tensile stress-crack width relationship for concrete.

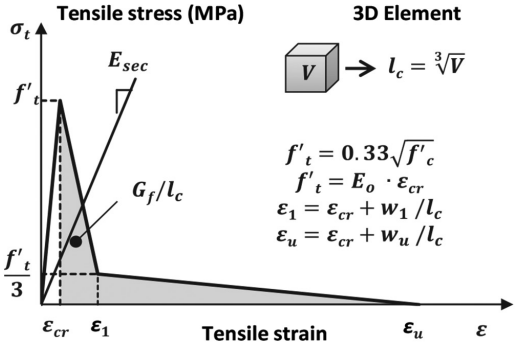

Fig. 4—Uniaxial tensile stress-strain relationship for concrete.

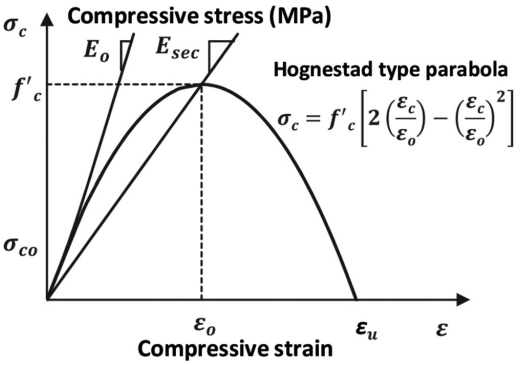

Fig. 5—Uniaxial compressive stress-strain relationship for concrete.

Concrete damaged plasticity model

Among other constitutive models for concrete (Simo and Ju 1987; Mazars and Pijaudier-Cabot 1989; Feenstra and de Borst 1996; Imran and Pantazopoulou 2001; Grassl et al. 2002), the concrete damaged plasticity model implemented in ABAQUS (2010) is adopted in this work. A short description of the constitutive modeling of concrete damaged plasticity model in ABAQUS (2010) is presented herein. The model includes two main failure mechanisms of concrete: 1) the tensile cracking; and 2) the compressive crushing. The yield function of the model was first suggested from Lubliner et al. (1988) and then in 1998 modified by Lee and Fenves. The general form of the yield function is described in Eq. (1) in terms of effective stresses

$$F = \frac{1}{1-\alpha}\left(\bar{q} - 3\alpha\bar{p} + \beta\left(\tilde{\varepsilon}^{pl}\right)\left\langle\hat{\bar{\sigma}}_{\max}\right\rangle - \gamma\left\langle\hat{\bar{\sigma}}_{\max}\right\rangle\right) - \bar{\sigma}_c\left(\tilde{\varepsilon}_c^{pl}\right) \tag{1}$$

The parameter α depends on the ratio of biaxial compressive strength (σ_{b0}) and uniaxial compressive strength (σ_{c0}) and it ranges between 0 and 0.5. A typical value for the ratio of biaxial compressive strength and uniaxial compressive strength for concrete is 1.16 and this value was adopted in this model. By specifying the stress ratio as 1.16 (default value in ABAQUS [2010]), the parameter α takes the value 0.1212. The yield function is defined in the $\bar{p} - \bar{q}$ plane, with $\bar{p}$ and $\bar{q}$ to be the effective stress tensor (hydrostatic pressure stress) and the Mises equivalent effective stress, respectively. The function $\beta\left(\tilde{\varepsilon}^{pl}\right)$ in Eq. (1) depends on parameter α and on the effective compressive $\bar{\sigma}_c\left(\tilde{\varepsilon}_c^{pl}\right)$ and tensile $\bar{\sigma}_t\left(\tilde{\varepsilon}_t^{pl}\right)$ cohesion stresses. Parameter γ defines the shape of the loading surface and the value that was given in this study was 2.94. The concrete damage plasticity model uses the non-associated Drucker-Prager hyperbolic function as the flow potential function, $G(\sigma)$, such as

$$G(\sigma) = \sqrt{\left(\varepsilon\sigma_{t0}\tan\psi\right)^2 + \bar{q}^2} - \bar{p}\tan\psi \tag{2}$$

where ε is the eccentricity that determines the rate at which the plastic potential function approaches the asymptote and σ_{t0} is the uniaxial tensile stress. The dilation angle ψ is measured in the $\bar{p} - \bar{q}$ plane and in this research was considered as 40 degrees after a calibration that has previously done in the model (Genikomsou and Polak 2015). The default value for the eccentricity was given (ε = 0.1). Tension in concrete is defined by a stress-fracture energy approach. The bilinear stress-crack displacement response proposed by Hillerborg et al. (1976) can be calculated as shown in Fig. 3. The stress-strain response is illustrated in Fig. 4. The critical length l_c in the simulations is 20 mm (0.79 in.) equal to the mesh size that was adopted in the analyses. The fracture energy G_f is obtained from the CEB-FIP Model Code 90 (1993) and the value of the fracture energy for each slab differs depending on the compressive strength of concrete and the aggregate size. The aggregate size was 10 mm (0.39 in.) for all slabs. The Hognestad-type parabola is used for describing the compressive behavior of concrete (Fig. 5). The uniaxial stress-strain relationship of reinforcement is modeled with a bilinear strain hardening yield stress-plastic strain curve. The elastic behavior of the reinforcement is defined by specifying the Young's modulus (E_s) and Poisson's ratio (ν). Table 3 summarizes the material and plasticity parameters for Slab XXX that have to be considered in ABAQUS (2010). It should be noted that the calibration of the FEA model is based on previous work on interior connections (Genikomsou and Polak 2015) and in this work on the Edge Specimen XXX. For other test specimens described in this paper, the calibrated model was used without any further changes (except for concrete strength and loading). For all analyzed slabs, the viscosity parameter μ (refer to Table 3) was considered equal to 0 because in

ABAQUS (2010) /Explicit, viscoplastic regularization is not required to converge the solution.

FINITE ELEMENT ANALYSIS RESULTS

Load-deflection responses

The test and FEA results for each specimen are described in Table 4 together with the ACI 318-14 predictions. The results obtained from the nonlinear FEA accurately describe the response of the tested slabs. The FEA of the slabs predicted the punching shear capacity is almost 10% lower compared to the test results. The experimental responses exhibited hardening before failure due to the loading protocol. These specimens were tested in load control mode and the load was slightly increased and then the slab failed. Finite element analysis would not capture this because finite element analyses are done using displacement increments. The FEA response of Slabs HXXX, HSE0, and CF0 appears stiffer compared to the response of the tests. This may happen due to the possible initial pre-cracking prior to the test (for example, shrinkage, handling). The same reason can be considered for the higher FEA ultimate load of Slabs HXXX and HSE0 compared to the test results. In both test and numerical results, the tensile reinforcement yielded first under the column. Cracking propagation in both test and FEA started on the tension side of the slabs. For specimens with ratio M/P = 0.3 m (11.81 in.), the cracking started at an approximately vertical load of 40 to 50 kN (8.99 to 11.24 kip) while for the specimens with ratio M/P = 0.66 m (25.98 in.), the cracks were initiated at a vertical load of 30 to 40 kN (6.74 to 8.99 kip). Cracking started from the inner corners of the columns and developed toward the edges of the slabs. Cracks on the compressive side of the slabs were developed at approximately 75% of the ultimate load for the specimens with ratio M/P = 0.3 m (11.81 in.). The specimens with ratio M/P = 0.66 m (25.98 in.) did not develop cracks on the compressive side of the slabs. It should be noted that the first cracks for Specimens SF0 and CF0 started from the inner corners of the openings and developed toward the edges of the slabs. The effect of the location of the opening size of 150 x 150 mm, in terms of the distance from the front column face on the punching shear capacity, was small for both test and FEA results. The comparison between Slabs SF0, SF1, and SF2, in terms of vertical load versus deflection, shows that Slab SF0 (with opening in front of the column on the right side) has the lower punching capacity. However, the differences were not significant. The opening is located at 90 and 180 mm from the front column face for Slabs SF1 and SF2, respectively. It is observed from both the test and analytical results that both slabs (SF1 and SF2) have almost the same response in terms of ultimate vertical load and displacement (Fig. 6(a) and (b)).

As illustrated in Fig. 6(c) and (d), the slab with the side face opening (SE0) has stiffer response compared to Slab SF0 that has opening in the front of the column face. In terms of ultimate load, Slab SE0 has approximately 10% higher ultimate load compared to Slab SF0 for both test and FEA. Figures 6(e) and (f) present the effect of the opening size. Three slabs are compared in terms of ultimate load and displacement. Slab XXX is the control specimen without opening; Slabs SF0 and CF0 have the openings located at the front column face, with size 150 x 150 mm and 250 x 250 mm (5.91 x 5.91 in. and 9.84 x 9.84 in.), respectively. Both experimental and analytical results showed that as the opening is increased, both stiffness and strength were reduced.

The effect of the unbalanced moments to the ultimate load is presented in Fig. 6(g) and (h). Slabs HXXX and HSF0 with

Table 3—Material properties and plasticity parameters of concrete for analysis of Slab XXX

Compressive strength of concrete f_c', MPa	33
Tensile strength of concrete f_t', MPa	$0.33\sqrt{f_c'} = 1.9$
Fracture energy of concrete G_f, mm	$G_{f0}(f_{cm}/f_{cmo})^{0.7} = 0.081$
Modulus of elasticity of concrete E_c, MPa	$5500\sqrt{f_c'} = 31{,}595$
Poisson's ratio ν	0.2
Dilation angle ψ, degrees	40
Eccentricity ε	0.1
Ratio of initial equibiaxial to initial uniaxial compressive yield stresses σ_{b0}/σ_{c0}	1.16
Ratio of stress invariants K_c	0.667
Viscosity parameter μ	0

Notes: 1 MPa = 0.145 ksi; 1 kN = 0.225 kip; 1 mm = 0.0394 in.

Table 4—*M/P* ratio, test and FEA results, and ACI predictions

		Test results		FEA results		ACI 318-14	
Slab specimen	M/P, m (in.)	Failure load, kN (kip)	Displacement at failure load, mm (in.)	Failure load, kN (kip)	Displacement at failure load, mm (in.)	Failure load, kN (kip)	F_{FEA}/F_{TEST}
XXX	0.3 (11.81in.)	125 (28.10)	15.06 (0.593)	112 (25.18)	17.69 (0.696)	88 (19.78)	0.896
SF0	0.3 (11.81in.)	110 (24.73)	15.95 (0.628)	97 (21.81)	14.94 (0.588)	56 (12.59)	0.882
SE0	0.3 (11.81in.)	120 (26.98)	15.55 (0.612)	109 (24.50)	17.75 (0.699)	78 (17.54)	0.908
SF1	0.3 (11.81in.)	115 (25.85)	15.02 (0.591)	102 (22.93)	14.57 (0.574)	70 (15.74)	0.887
SF2	0.3 (11.81in.)	114 (25.63)	13.44 (0.529)	106 (23.83)	13.74 (0.541)	72 (16.19)	0.930
CF0	0.3 (11.81in.)	86 (19.33)	11.01 (0.433)	86 (19.33)	12.75 (0.502)	33 (7.42)	1.000
HXXX	0.66 (25.98 in.)	69 (15.51)	5.96 (0.235)	84 (18.88)	6.77 (0.266)	54 (12.14)	1.217
HSF0	0.66 (25.98 in.)	58 (13.04)	6.95 (0.274)	60 (13.49)	6.93 (0.273)	33 (7.42)	1.034
HSE0	0.66 (25.98 in.)	65 (14.61)	5.26 (0.207)	76 (17.09)	6.23 (0.245)	53 (11.91)	1.170

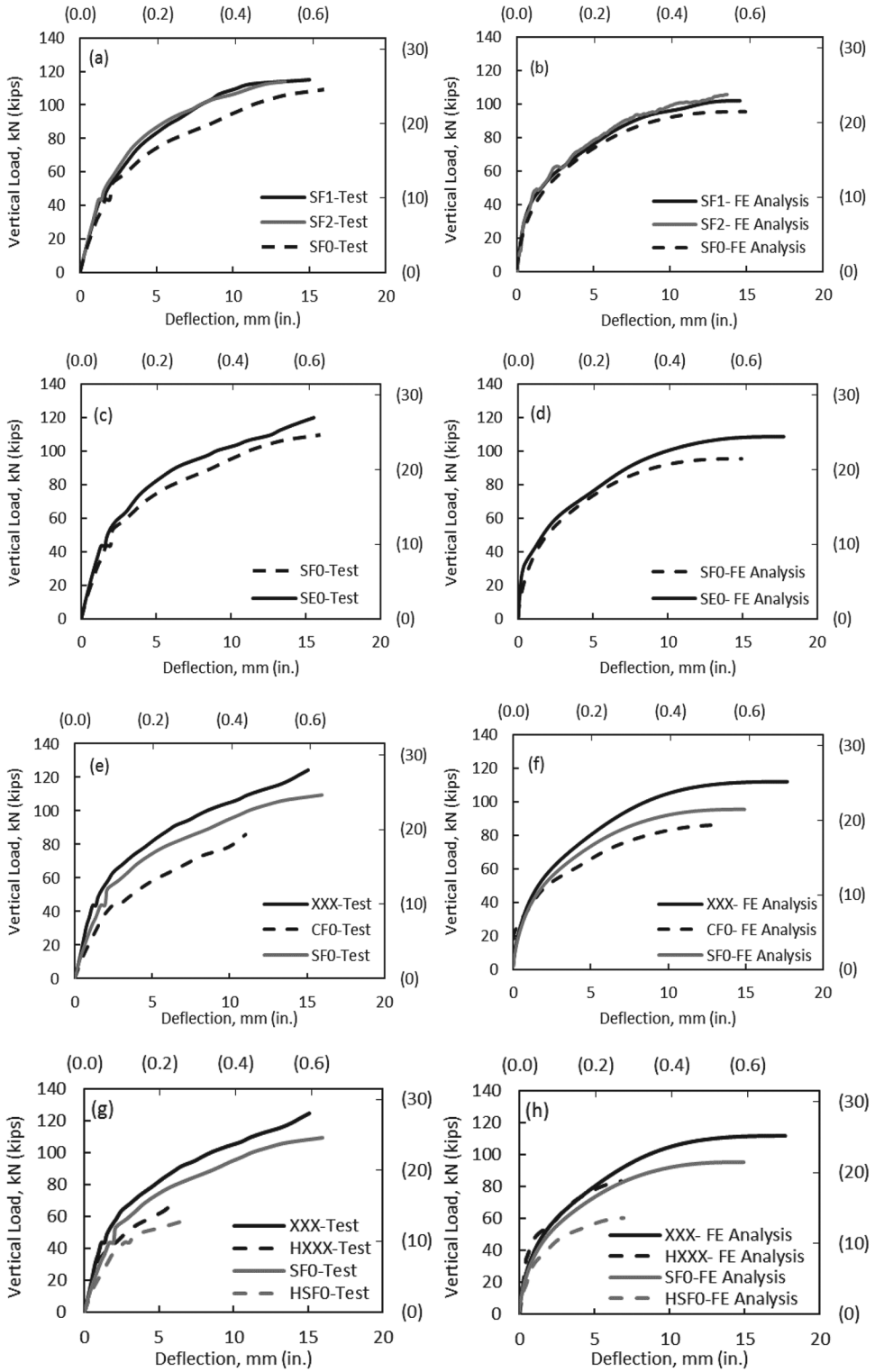

Fig. 6—Comparison between numerical and test results in terms of vertical load deflection.

unbalanced moment to shear force ratio 0.66 m (25.98 in.) are compared to Slabs XXX and SF0 with unbalanced moment to shear force ratio 0.3 m (11.81 in.), for both tested and analytical results. Slab HXXX had lower tested punching shear capacity (approximately 50% less) compared to Slab XXX. The FEA showed that the punching shear capacity of Slab HXXX was 25% lower compared to Slab XXX. The tested slab HSF0 had lower punching shear capacity (approximately 47%) compared to the tested slab SF0. The finite element simulations showed that the punching shear capacity of Slab HSF0 was 38% lower compared to Slab SF0.

Design provisions according to ACI 318-14

Based on the results presented in Table 4, ACI 318-14 appears to provide conservative predictions. Especially for the slabs with openings, ACI 318-14 predicts much lower punching shear loads compared to the results from the tests

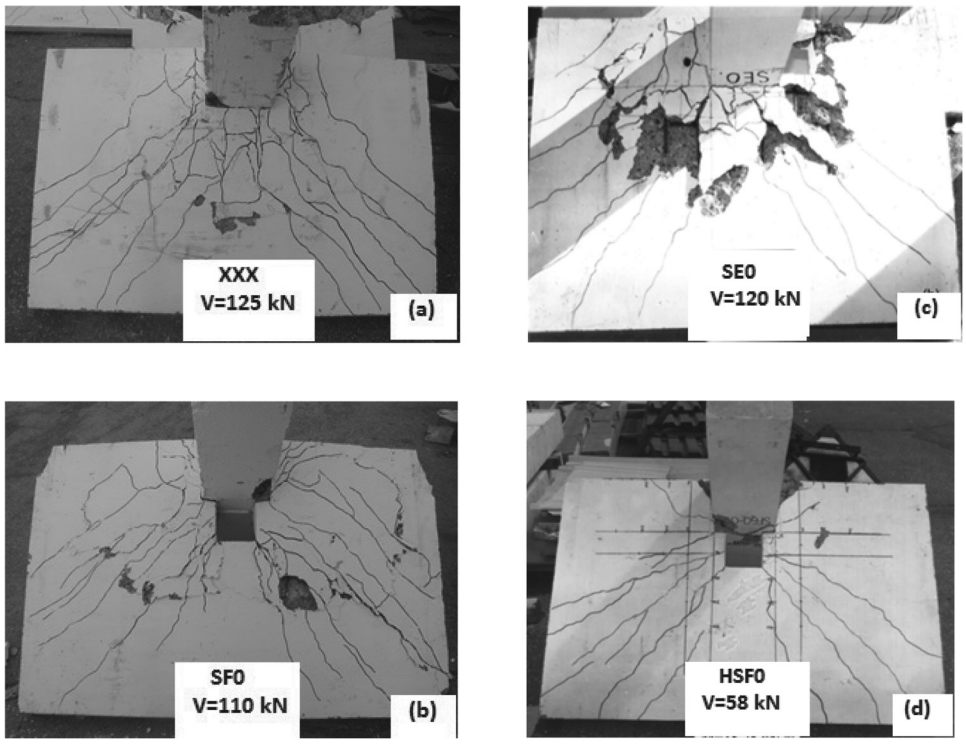

Fig. 7—Crack patterns at ultimate load (El-Salakawy et al. 1999). (Note: 1 kN = 0.225 kip.)

and the FEA. ACI 318-14, which is based on Moe's (1961) research, considers the critical section at distance 0.5*d* (*d* is the effective depth of the slab) from the column perimeter to calculate the shear capacity of the slab. For slabs under gravity load and connection moment *M*, the shear stress on critical perimeter in ACI 318-14 is calculated

$$v_f = \frac{V_f}{b_o d} + \frac{\gamma_v M_f c}{J_c} \tag{3}$$

where v_f is the factored shear stress; V_f is the vertical factored shear force; b_o is the control perimeter; d is the effective depth of the slab; J_c is the property of critical section, which is analogous to the polar moment of inertia;

$$\gamma_v = 1 - \frac{1}{1 + \frac{2}{3}\sqrt{\frac{b_1}{b_2}}}$$

is the fraction of the unbalanced moment transferred by shear eccentricity, where b_1 is the width of the critical section perpendicular to the moment vector and b_2 is the other side length and c is the centroid of the critical perimeter section.

According to ACI 318-14, the punching shear stress of the slabs without shear reinforcement (v_f) is

$$v_c = \min \begin{cases} 0.33\lambda\sqrt{f_c'} \\ 0.17\lambda\sqrt{f_c'}\left(1 + \frac{2}{\beta_c}\right) \\ 0.083\lambda\sqrt{f_c'}\left(2 + \frac{\alpha_s d}{b_o}\right) \end{cases} \quad (f_c' \text{ in MPa}) \tag{4}$$

where λ is the concrete density factor equal with 1 for a normalweight concrete; f_c' is the compressive strength of concrete; β_c is the ratio of the long to short side of the column; and α_s is 40 for interior columns, 30 for edge columns, and 20 for corner columns.

Cracking propagation

Figure 7 and 8 illustrate the crack pattern at the bottom surface of some selected slabs at failure, as it was observed from the tests and the cracking of the same slabs as it was observed from the FEA, respectively. The cracking in concrete damaged plasticity model can be illustrated through the maximum principal plastic strains. It becomes obvious by comparing Fig. 7 and 8 that all crack patterns obtained from the finite element simulations are in good agreement with the cracking propagation observed from the tests.

The crack patterns of Slabs SF0, SF1, and SF2 at failure are presented in Fig. 9. These three slabs had the same size of openings (150 x 150 mm [5.91 x 5.91 in.]) in front of the column but at different distances from the column. These slabs had similar ultimate loads and deflections but different crack patterns. The cracking propagation could be presented into three loading stages for the FEA results. Up to 40% of the ultimate load (Fig. 9(a)), the cracking is concentrated around the column with some radial cracks on the tension side on the diagonal. It is quite interesting to notice that this diagonal cracks in the case of Specimens SF0 and SF1 start to develop at the corner of the opening, while for Specimen SF2 start to develop at the corner of the column. At the 80% of the ultimate load (Fig. 9(b)), the shear cracks have already developed and extended further, and tangential cracks have developed and continued to the diagonal of the slab. At this load stage, more radial cracks become visible.

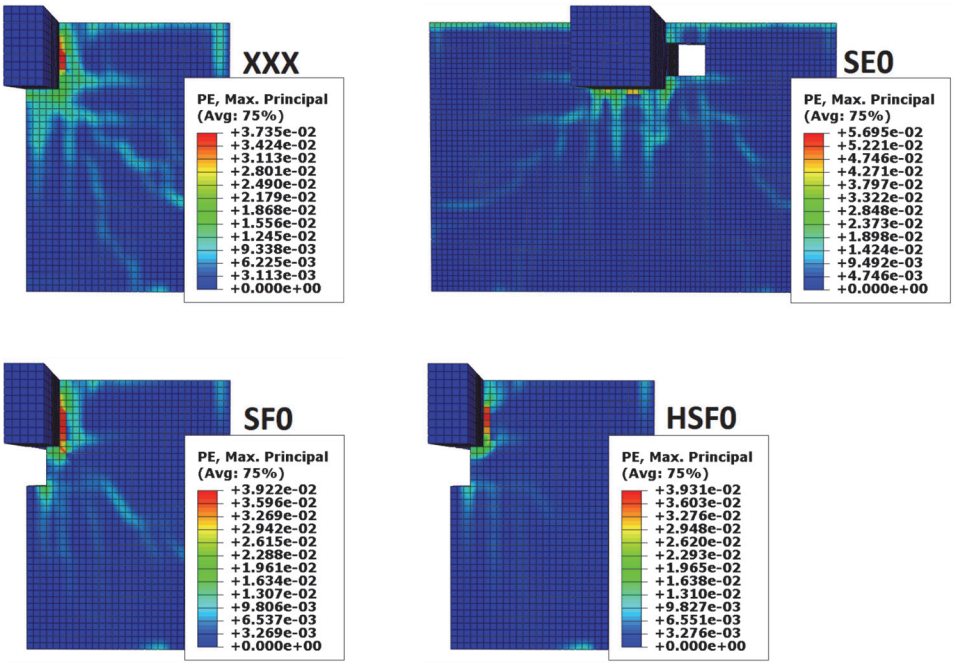

Fig. 8—Crack patterns from FEA at failure.

Finally, at the ultimate load (Fig. 9(c)), the shear cracks open suddenly. Cracks of the slab SF1 form next to the column with secondary cracks that develop from the corner of the opening. However, the cracks of Specimen SF2 do not develop past the opening.

Parametric investigation—effect of opening location and size

The calibrated FEA model presented herein is used to develop an extended parametric study. Two previously shown edge specimens (SF0 and CF0) and an interior slab-column connection (SB1) are used as the reference slabs for the parametric analyses to investigate the effect of the opening location and size on the punching shear capacity. In all analyzed slabs, the amount of the flexural reinforcement that is cut due to the creation of openings is replaced by adding an equivalent reinforcement along the four sides of the square openings. With this way, the reinforcement ratio of the slabs was the same with the reference slabs that have no openings. The selected opening sizes are based on the limited size of the investigated slabs. The support conditions may influence the cases in both types of slabs (edge and interior) when the openings are located at distance 4*d* (450 mm [17.7 in.]) from the face of the column; their sizes are 250 and 200 mm (9.8 and 7.8 in.) for the edge and interior slabs, respectively. However, because the effect of the openings is not significant in the FEA at a distance 3*d*, it is also expecting to not be significant at further distances. Future studies should examine larger slabs to consider larger openings without a limitation of the support conditions.

Edge slab-column connections—Figure 10 presents the parametric study of the edge specimens. The previously shown Slabs SF0, SF1, SF2, and CF0 are considered as the reference slabs for the analyses. The opening effect is examined when it exists in front of the column and not beside it because this was found as the worst scenario in both the test and numerical results (refer to the responses of Slabs SF0 and SE0). Opening size and distance from the column were studied. Two opening sizes were considered: 150 x 150 mm (5.91 x 5.91 in.) and 250 x 250 mm (9.84 x 9.84 in.). The distance of these openings from the column varied from 0*d* to 5*d* (450 mm), where *d* is the effective depth of the slab equal to 90 mm (3.54 in.). Figure 11 presents the effect of the opening location and size for the slabs. The FEA results showed that as the opening was located further from the column face, the punching shear capacity of the slab was increased. If the opening is located further than the distance 4*d* (360 mm [14.17 in.]), the strength of the slab becomes almost the same as for the specimen that has no opening (XXX). Also, the difference in the ultimate loads between the slabs with the smaller and larger openings seems to not be significant after the distance 4*d*. Therefore, based on these results, reduction of the slab's strength due to openings should be considered when the opening is located at a distance less than 4*d* from the column. Figure 11 compares the predictions from ACI 318-14 with the FEA results. ACI is conservative for all analyzed slabs. Regarding the opening size, ACI predicts different failure loads for Slabs SF5 and CF5 compared to the FEA results that show the same punching shear resistance for both slabs. Table 5 summarizes the obtained results from the parametric study and the ACI 318-14 code predictions in terms of ultimate load.

Interior slab-column connections—Figure 12 shows the interior slab-column connections that were considered for parametric investigation. The analyzed specimens were same as Specimen SB1 (except for the openings in the slabs). SB1 was tested under gravity load through the column (Adetifa and Polak 2005). The dimensions of SB1 were 1800 x 1800 mm (70.87 x 70.87 in.) with simple supports at 1500 x 1500 mm (59.06 x 59.06 in.). The height and the effective depth of the slab were 120 and 90 mm (4.72 and 3.54 in.), respectively. The square column (150 x 150 mm [5.91 x

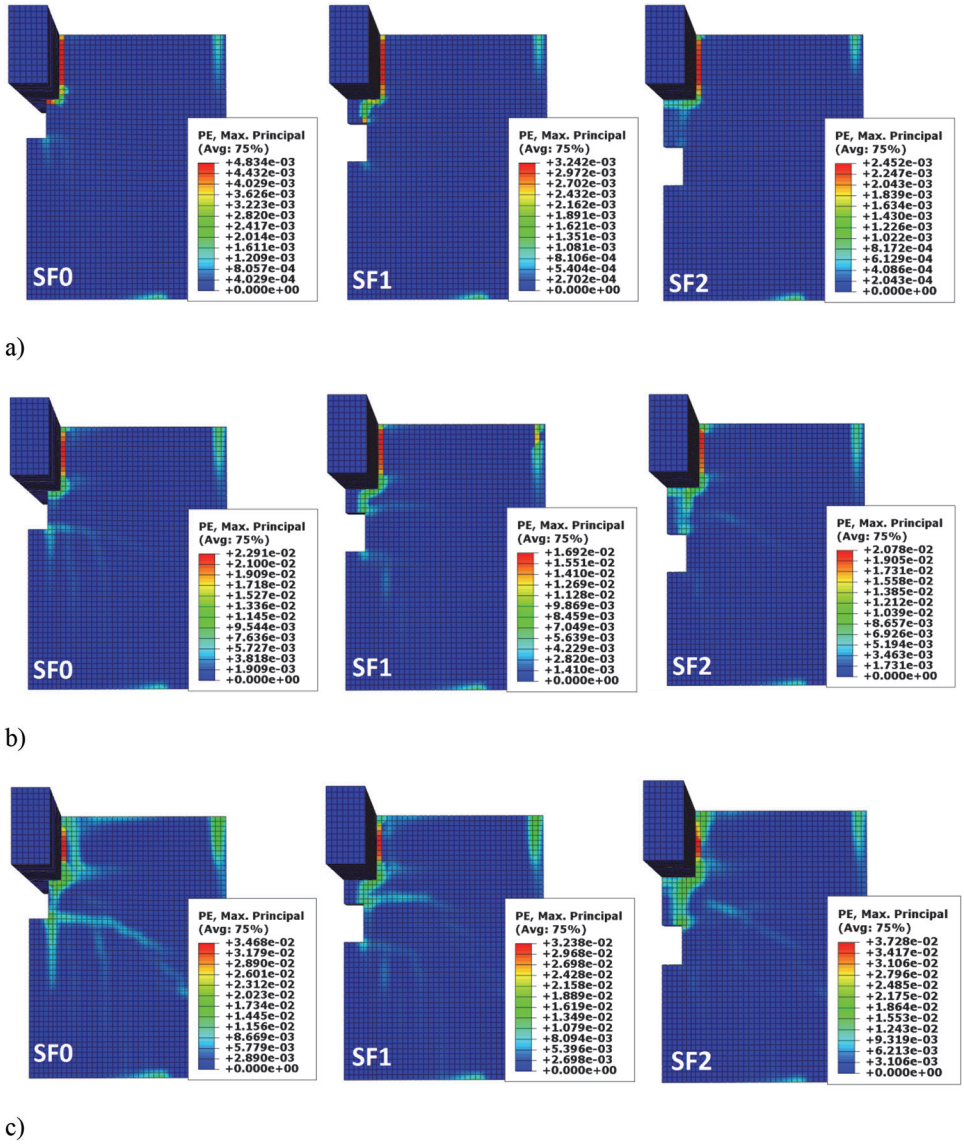

Fig. 9—Cracking propagation of Slabs SF0, SF1, and SF2: (a) 40% of ultimate load; (b) 80% of ultimate load; and (c) ultimate load.

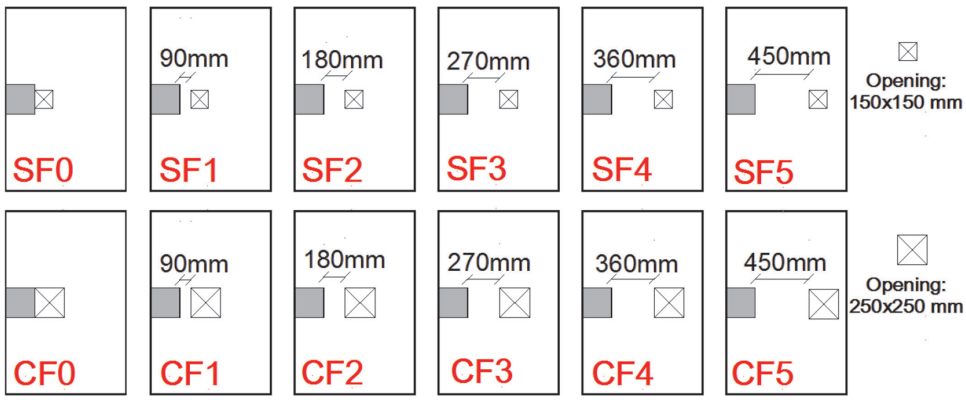

Fig. 10—Schematic drawing of edge slabs with openings. (Note: 1 mm = 0.0394 in.)

5.91 in.]) was extended 150 mm (5.91 in.) from the top and the bottom surfaces of the slab. The compressive strength of the concrete was 44 MPa. The bars of the tension flexural reinforcement were 10M with spacing 100 and 90 mm (3.94 and 3.54 in.) for the lower and upper layers, respectively, and the bars of the compressive flexural reinforcement were 10M with a spacing of 200 mm (7.87 in.) for both the top and bottom layers. During the test, Slab SB1 failed in punching shear at a load of 253 kN (56.88 kip). The FEA results showed the punching shear failure at a load of 216 kN (48.56 kip).

Five opening sizes are considered for the parametric studies: 50 x 50 mm (1.97 x 1.97 in.), 70 x 70 mm (2.76 x 2.76 in.), 100 x 100 mm (3.94 x 3.94 in.), 150 x 150 mm (5.91 x 5.91 in.), and 200 x 200 mm (7.87 x 7.87 in.). Due to symmetry, one quarter of Slab SB1 is analyzed; thus, two openings are considered in each case study. The distance of these openings from the face of the column ranges from 0 to 450 mm (17.72 in.); 450 mm = 5*d*, where *d* is the effective depth of the slab equal to 90 mm (3.54 in.).

Figure 13 presents the effect of the opening location and size for the interior slab-column connections. The FEA results show that as the opening is located further to the column, the punching shear capacity of the slab increases. When the opening is located after the distance 4*d* (360 mm [14.17 in.]), the strength of the slab becomes almost the same with the specimen that has no opening (SB1). Also, the difference in the ultimate loads between the slabs with the smaller and larger openings seems to be not significant after the distance 3*d*. When the opening is located at a distance 5*d* from the column it does not affect the punching shear capacity of the slab, regardless of the opening size. Therefore, reduction of slab's strength due to openings should be considered when the opening is located at a distance less than 4*d* from the column. The predictions from ACI 318-14 are conservative for all analyzed slabs, even if the opening is located at a distance 5*d* from the column. The size of the openings affects the predicted punching shear capacity. Table 6 summarizes the obtained results from the parametric study and the ACI 318-14 code predictions in terms of ultimate load for the interior slab-column connections. The punching shear resistance of the slabs V_c according to ACI 318-14 is obtained from Eq. (4). Figure 14 presents the cracking at the failure load for six interior slab-column connections, where three different opening sizes are shown (50, 100, and 200 mm [1.97, 3.94, and 7.87 in.]) located at distances 0*d*, 2*d*, and 4*d*. The cracks for slabs with different opening sizes but located at distance 4*d* are the same, regardless of the opening size.

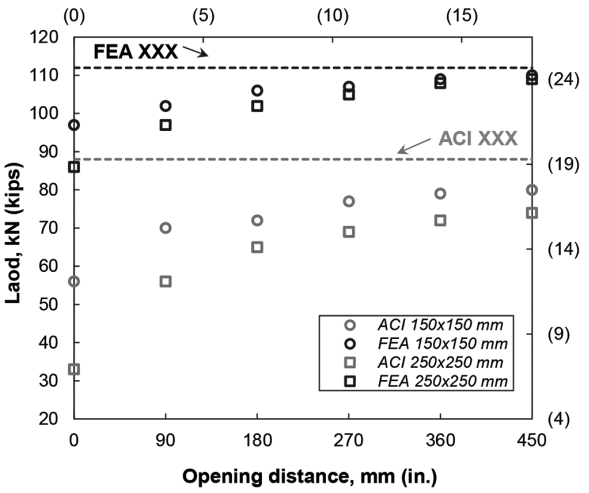

Fig. 11—Distance effect on punching shear resistance for edge slabs.

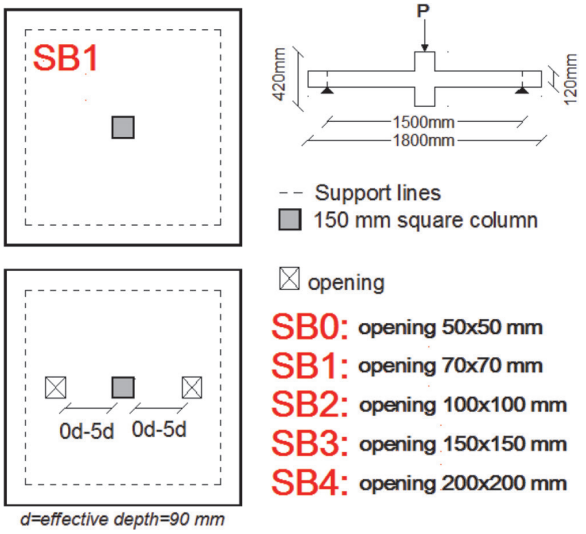

Fig. 12—Schematic drawing of interior slabs with openings. (Note: 1 mm = 0.0394 in.)

Table 5—Comparison between FEA results and ACI predictions for edge slabs

Slab specimen	f_c', MPa (ksi)	Opening distance from column	Opening size, mm (in.)	FEA punching shear load, kN (kip)	ACI 318-14 punching shear load, kN (kip)
SF0	31.5 (4.57)	0*d*	150 x 150 (5.91 x 5.91)	97 (21.81)	56 (12.59)
CF0	30.5 (4.42)		250 x 250 (9.84 x 9.84)	86 (19.33)	33 (7.42)
SF1	33 (4.79)	1*d* = 90 mm	150 x 150 (5.91 x 5.91)	102 (22.93)	70 (15.74)
CF1	30.5 (4.42)		250 x 250 (9.84 x 9.84)	97 (21.81)	56 (12.59)
SF2	30 (4.35)	2*d* = 180 mm	150 x 150 (5.91 x 5.91)	106 (23.83)	72 (16.19)
CF2	30.5 (4.42)		250 x 250 (9.84 x 9.84)	102 (22.93)	65 (14.61)
SF3	31.5 (4.57)	3*d* = 240 mm	150 x 150 (5.91 x 5.91)	107 (24.05)	77 (17.31)
CF3	30.5 (4.42)		250 x 250 (9.84 x 9.84)	105 (23.60)	69 (15.51)
SF4	31.5 (4.57)	4*d* = 360 mm	150 x 150 (5.91 x 5.91)	109 (24.50)	79 (17.76)
CF4	30.5 (4.42)		250 x 250 (9.84 x 9.84)	108 (24.28)	72 (16.19)
SF5	31.5 (4.57)	5*d* = 450 mm	150 x 150 (5.91 x 5.91)	110 (24.73)	80 (17.98)
CF5	30.5 (4.42)		250 x 250 (9.84 x 9.84)	109 (24.50)	74 (16.64)

Note: *d* is effective depth of slab = 90 mm ≈ 3.54 in.; 1 mm = 0.0394 in.

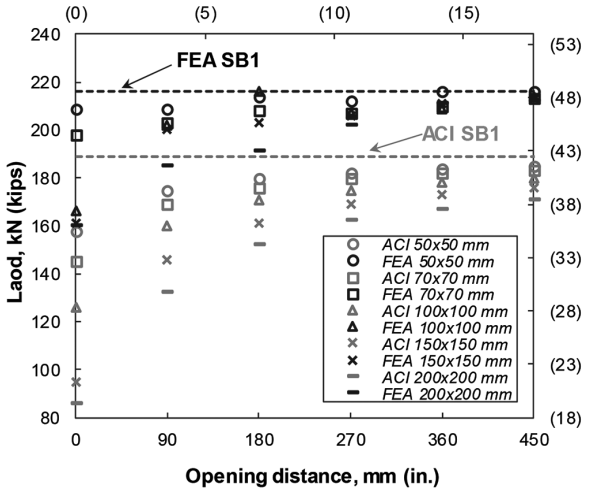

Fig. 13—Distance effect on punching shear resistance for interior slabs.

CONCLUSIONS

Finite element analyses (FEA) were performed to extend the existing experimental database for punching shear strength of reinforced concrete slabs with openings. Nonlinear finite element analysis of RC structures can, however, be very helpful to see the trends and the effects that certain parameters have on the structural response. In this work, the nonlinear FEA is treated as a tool that can help in the development of design provisions, not a design tool for structures. The analyses were done using calibrated finite element models because nonlinear FEA is not a tool that can be adopted blindly for analysis of RC structures. Based on the work presented in this paper, the following conclusions can be offered:

1. The concrete damaged plasticity model in ABAQUS can be effectively used for the analysis of slabs with openings located near the column that fail in punching shear.

Table 6—Comparison between FEA results and ACI predictions for interior slabs

Slab specimen	Opening distance from column	Opening size, mm (in.)	FEA punching shear load, kN (kip)	ACI 318-14 punching shear load, kN (kip)
SB0-0		50 x 50 (1.97 x 1.97)	209 (46.99)	158 (35.52)
SB1-0		70 x 70 (2.76 x 2.76)	198 (44.51)	145 (32.60)
SB2-0	0*d*	100 x 100 (3.94 x 3.94)	166 (37.32)	126 (28.33)
SB3-0		150 x 150 (5.91 x 5.91)	161 (36.19)	95 (21.36)
SB4-0		200 x 200 (7.87 x 7.87)	160 (35.97)	86 (19.33)
SB0-1		50 x 50 (1.97 x 1.97)	209 (46.99)	175 (39.34)
SB1-1		70 x 70 (2.76 x 2.76)	203 (45.64)	169 (37.99)
SB2-1	1*d*	100 x 100 (3.94 x 3.94)	202 (45.41)	160 (35.97)
SB3-1		150 x 150 (5.91 x 5.91)	203 (45.64)	146 (32.82)
SB4-1		200 x 200 (7.87 x 7.87)	185 (41.59)	132 (29.67)
SB0-2		50 x 50 (1.97 x 1.97)	214 (48.11)	180 (40.47)
SB1-2		70 x 70 (2.76 x 2.76)	208 (46.76)	176 (39.57)
SB2-2	2*d*	100 x 100 (3.94 x 3.94)	216 (48.56)	171 (38.44)
SB3-2		150 x 150 (5.91 x 5.91)	203 (45.64)	161 (36.19)
SB4-2		200 x 200 (7.87 x 7.87)	191 (42.94)	152 (34.17)
SB0-3		50 x 50 (1.97 x 1.97)	212 (47.66)	182 (40.92)
SB1-3		70 x 70 (2.76 x 2.76)	207 (46.54)	180 (40.47)
SB2-3	3*d*	100 x 100 (3.94 x 3.94)	207 (46.54)	175 (39.34)
SB3-3		150 x 150 (5.91 x 5.91)	206 (46.31)	169 (37.99)
SB4-3		200 x 200 (7.87 x 7.87)	202 (45.41)	162 (36.42)
SB0-4		50 x 50 (1.97 x 1.97)	216 (48.56)	184 (41.36)
SB1-4		70 x 70 (2.76 x 2.76)	210 (47.21)	182 (40.92)
SB2-4	4*d*	100 x 100 (3.94 x 3.94)	209 (46.99)	178 (40.02)
SB3-4		150 x 150 (5.91 x 5.91)	211 (47.43)	173 (38.89)
SB4-4		200 x 200 (7.87 x 7.87)	211 (47.43)	167 (37.54)
SB0-5		50 x 50 (1.97 x 1.97)	216 (48.56)	185 (41.59)
SB1-5		70 x 70 (2.76 x 2.76)	213 (47.88)	183 (41.14)
SB2-5	5*d*	100 x 100 (3.94 x 3.94)	214 (48.11)	180 (40.47)
SB3-5		150 x 150 (5.91 x 5.91)	213 (47.88)	176 (39.57)
SB4-5		200 x 200 (7.87 x 7.87)	212 (47.66)	171 (38.44)

Note: *d* is effective depth of slab = 90 mm ≈ 3.54 in.

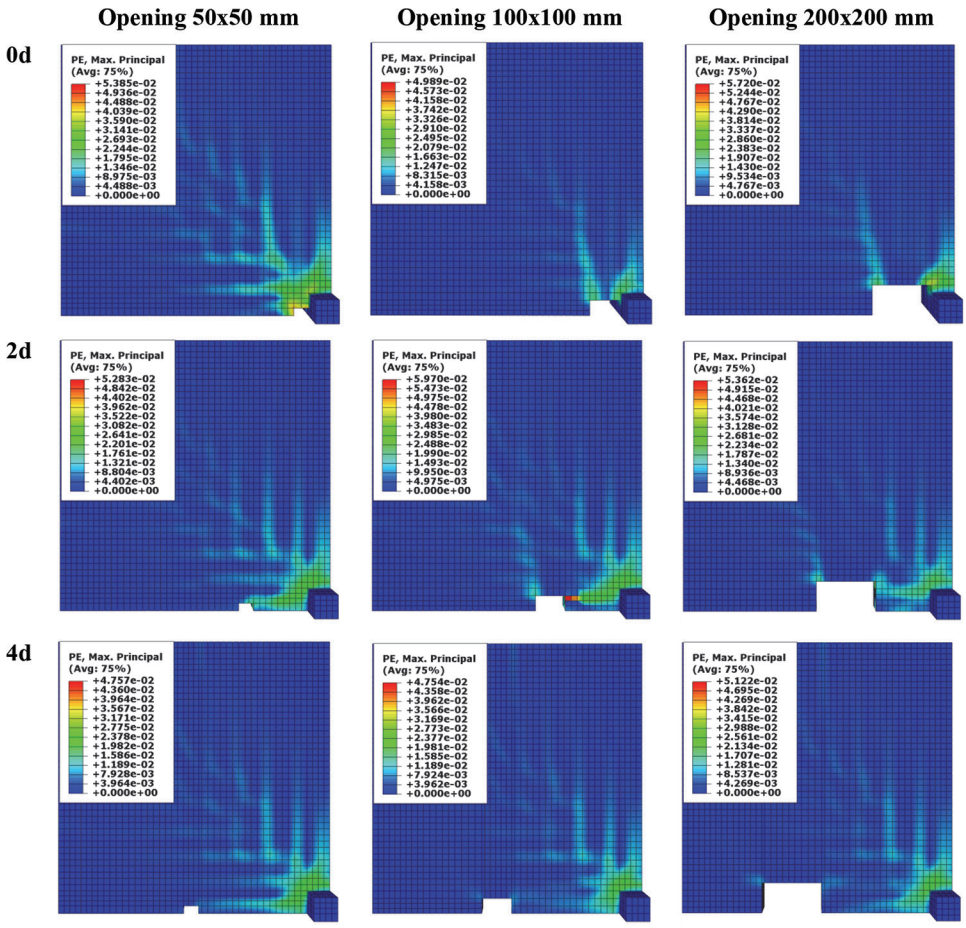

Fig. 14—Crack pattern for interior slab-column connections.

However, the effectiveness of the FEA should be established by comparisons of the numerical crack patterns and ultimate loads to the experimental results.

2. The openings in concrete flat slabs reduce the punching shear strength of the slabs. This reduction depends on the distance of the opening from the face of the column and size of the opening. However, the experimental results of the edge specimens showed similar failure loads for the SF1 slab (opening at distance 1*d* from the column) and SF2 slab (opening at distance 2*d* from the column). Slab SF1 failed at a load of 115 kN, while Slab SF2 failed at a load of 114 kN. This test observation was the basis for the presented parametric studies in this research.

3. The results from the parametric investigations have shown that when the opening is located at a distance larger than 4*d* from the column, the punching shear capacity of the slab remains the same as for the slab without openings. For small openings (50 and 70 mm [1.9 and 2.76 in.]), the punching shear capacity of the interior slabs was the same as for the specimen that has no openings when the openings were located at distance 2*d* from the column. Based on the FEA parametric studies, it can be also said that the size of the opening does play significant role to the reduction of the punching shear load (when the opening is larger) if the opening is located next to the column (at distance 0*d*). The influence of the size of the opening is not significant when the opening is located after the distance 3*d* from the face of the column.

4. The main advantage of the FEA is that they can give an insight into the slabs' behavior by showing the crack propagation. The propagation of cracking shows that the cracks in the slabs with openings next to the column propagate starting from the columns and around the opening (SF0). In the cases where the openings are located at a distance from the column (*d* and 2*d* for SF1 and SF2, respectively), secondary cracks form and start to propagate from the corners of the openings and extend away from the columns. Similar observations are noticed for the interiors slabs.

5. ACI 318-14 gives safe results compared to the test and numerical observations, but in all cases ACI 318-14 underestimates the punching shear capacity of the slabs. The conservatism of ACI 318-14 becomes more significant when slabs have openings. The largest difference between the FEA results and the ACI 318-14 predicted loads is found when the openings are located next to the column.

AUTHOR BIOS

ACI member **Aikaterini S. Genikomsou** *is an Assistant Professor in the Department of Civil Engineering at Queen's University, Kingston, ON, Canada. She received her doctoral degree in civil engineering from the University of Waterloo, Waterloo, ON, Canada. Her research interests include the mechanics and constitutive modeling of reinforced concrete, punching shear design, novel materials in structural connections, and finite element analysis.*

Maria Anna Polak, *FACI, is a Professor in the Department of Civil and Environmental Engineering at the University of Waterloo. She is a member of ACI Committees 435, Deflection of Concrete Building Structures, and 440, Fiber-Reinforced Polymer Reinforcement, and Joint ACI-ASCE Committee*

445, Shear and Torsion. Her research interests include mechanics of reinforced concrete structures, nonlinear finite element analysis, and constitutive modeling of materials.

ACKNOWLEDGMENTS

The authors would like to acknowledge the financial support for the presented work provided by a research grant from the Natural Sciences and Engineering Research Council (NSERC) of Canada.

REFERENCES

ABAQUS, 2010, *Analysis User's Manual 6.10EF*, Dassault Systems Simulia Corp., Providence, RI.

ACI Committee 318, 2014, "Building Code Requirements for Structural Concrete (ACI 318-14) and Commentary (ACI 318R-14)," American Concrete Institute, Farmington Hills, MI, 2014, pp. 93-128.

Adetifa, B., and Polak, M. A., 2005, "Retrofit of Slab Column Interior Connections Using Shear Bolts," *ACI Structural Journal*, V. 102, No. 2, Mar.-Apr. pp. 268-274.

Anil, O.; Kina, T.; and Salmani, V., 2014, "Effect of Opening Size and Location on Punching Shear Behaviour of Two-Way RC Slabs," *Magazine of Concrete Research*, V. 66, No. 18, pp. 955-966.

Borges, L. L. J.; Melo, G. S.; and Gomes, R. B., 2013, "Punching Shear of Reinforced Concrete Flat Plates with Openings," *ACI Structural Journal*, V. 110, No. 4, July-Aug., pp. 547-556.

Bu, W., and Polak, M. A., 2009, Seismic Retrofit of Reinforced Concrete Slab-Column Connections using Shear Bolts," *ACI Structural Journal*, V. 106, No. 4, July-Aug., pp. 514-522.

Comité Euro-International du Béton, 1993, "CEB-FIP Model Code 1990: Design Code," Thomas Telford, London, UK, pp. 33-37.

El-Salakawy, E. F.; Polak, M. A.; and Soliman, M. H., 1999, "Reinforced Concrete Slab-Column Edge Connections with Openings," *ACI Structural Journal*, V. 96, No. 1, Jan.-Feb., pp. 79-87.

Elstner, R. C., and Hognestad, E., 1956, "Shearing Strength of Reinforced Concrete Slabs," *ACI Journal Proceedings*, V. 53, No. 7, July, pp. 29-58.

Feenstra, P. H., and de Borst, R., 1996, "A Composite Plasticity Model for Concrete," *International Journal of Solids and Structures*, V. 33, No. 5, pp. 707-730.

Genikomsou, A. S., and Polak, M. A.2015 , "Finite Element Analysis of Punching Shear of Concrete Slabs Using Damaged Plasticity Model in ABAQUS," *Engineering Structures*, V. 98, No. 4, pp. 38-48.

Grassl, P.; Lundgren, K.; and Gylltoft, K., 2002, "Concrete in Compression: A Plasticity Theory with a Novel Hardening Law," *International Journal of Solids and Structures*, V. 39, No. 20, pp. 5205-5223.

Guan, H., and Polak, M. A., 2007, "Finite Element Studies of Reinforced Concrete Slab-Edge Column Connections with Opening," *Canadian Journal of Civil Engineering*, V. 34, No. 8, pp. 952-965.

Ha, T.; Lee, M.-H.; Park, J.; and Kim, D.-J., 2015, "Effects of Openings on the Punching Shear Strength of RC Flat-Plate Slabs without Shear Reinforcement," *Structural Design of Tall and Special Buildings*, V. 24, pp. 895-911.

Hillerborg, A., 1985, "The Theoretical Basis of a Method to Determine the Fracture Energy G_F of Concrete," *Materials and Structures*, V. 18, No. 4, pp. 291-296.

Hillerborg, A.; Modéer, M.; and Petersson, P. E., 1976, "Analysis of Crack Formation and Crack Growth in Concrete by Means of Fracture Mechanics and Finite Elements," *Cement and Concrete Research*, V. 6, No. 6, pp. 773-781.

Hognested, E.; Elstner, R. C.; and Hanson, J. A., 1964, "Shear Strength of Lightweight Aggregate Concrete Slabs," *ACI Journal Proceedings*, V. 61, No. 6, June, pp. 643-656.

Imran, I., and Pantazopoulou, S. J., 2001, "Plasticity Model for Concrete under Triaxial Compression," *Journal of Engineering Mechanics*, V. 127, No. 3, pp. 281-290.

Joint ACI-ASCE Committee 326, "Shear and Diagonal Tension," *ACI Journal Proceedings*, V. 56, No. 3, Mar. 1962, pp. 356-396.

Lee, J., and Fenves, G. L., 1998, "Plastic-Damage Model for Cyclic Loading of Concrete Structures," *Journal of Engineering Mechanics*, V. 124, No. 8, pp. 892-900.

Lubliner, J.; Oliver, J.; Oller, S.; and Oñate, E., 1988, "A Plastic-Damage Model for Concrete," *International Journal of Solids and Structures*, V. 25, No. 3, pp. 299-326.

Mazars, J., and Pijaudier-Cabot, G., 1989, "Continuum Damage Theory—Application to Concrete," *Journal of Engineering Mechanics*, V. 115, No. 2, pp. 345-365.

Moe, J., 1961, "Shearing Strength of Reinforced Concrete Slabs and Footings under Concentrated Loads," *Development Department Bulletin D47*, Portland Cement Association, Skokie, IL.

Mowrer, R. D., and Vanderbilt, M. D., 1967, Shear Strength of Lightweight Aggregate Reinforced Concrete Flate Plates," *ACI Journal Proceedings*, V. 64, No. 11, pp. 722-729.

Roll, F.; Zaidi, S. T. H.; Sabnis, G.; and Chuang, K., 1971, "Shear Resistance of Perforated Reinforced Concrete Slabs," *Cracking, Deflection and Ultimate Load of Concrete Slab Systems*, SP-30, American Concrete Institute, Farmington Hills, MI, pp. 77-101.

Simo, J. C., and Ju, J. W., 1987, "Strain- and Stress-Based Continuum Damage Model—I. Formulation," *International Journal of Solids and Structures*, V. 23, No. 7, pp. 821-840.

Teng, S.; Cheong, H. K.; Kuang, K. L.; and Geng, J. Z., 2004, "Punching Shear Strength of Slabs with Openings and Supported on Rectangular Columns," *ACI Structural Journal*, V. 101, No. 5, Sept.-Oct., pp. 678-687.

Vanderbilt, M. D., 1972, "Shear Strength of Flat Plates," *Journal of the Structural Division*, ASCE, V. 98, pp. 961-973.

ACI Research and Academic Opportunities

This article details some of the opportunities for researchers and professionals upon becoming a part of the ACI community. This article will outline the possibilities available to members, such as attending The ACI Concrete Convention and Exposition, viewing past technical presentations, access to a vast abstract library, and ACI's Call for Papers. Up-to-date information concerning these and additional opportunites can be found at ACI's website, www.concrete.org.

THE ACI CONCRETE CONVENTION AND EXPOSITION

ACI Conventions give attendees the opportunity to participate in the development of industry codes and standards, learn about the latest in concrete technology, network with leading concrete professionals, and fulfill potential continuing education requirements.

ACI technical and educational sessions, which are held during ACI Conventions, provide attendees with the latest research, case studies, best practices, and opportunities to earn Professional Development Hours and Continuing Education Units. ACI committees, whose meetings take place during the ACI Convention, develop the standards, reports, and other documents needed to keep those in the industry up to date with the latest technology. Committee meetings are open to all registered convention attendees.

The ACI Convention takes place twice a year—once in the fall and once in the spring. ACI reserves rooms at local hotels and offers a discounted rate to members. Networking and other nontechnical events are coordinated through ACI and take place at each convention.

ACI Convention Schedule

City	Location	Dates
Anaheim, CA, USA	Disneyland Hotel	October 15-19, 2017
Salt Lake City, UT, USA	Grand America & Little America	March 25-29, 2018
Las Vegas, NV, USA	Rio All-Suites Hotel & Casino	October 14-18, 2018
Quebec City, QC, Canada	Quebec City Convention Centre & Hilton Hotel	March 24-28, 2019
Cincinnati, OH, USA	Duke Energy Convention Center & Hyatt Regency Cincinnati	October 20-24, 2019
Rosemont, IL, USA	Hyatt Regency O'Hare	March 29-April 2, 2020
Raleigh, NC, USA	Raleigh Convention Center & Raleigh Marriott	October 25-29, 2020
Baltimore, MD, USA	Hilton & Marriott Baltimore	March 28-April 1, 2021

TECHNICAL PRESENTATIONS AND DOCUMENTS

Access to a vast abstract library, online educational presentations, webinars, and ACI education documents are often free for members or offered at a discounted rate. New presentations and documents are always being added.

CALL FOR PAPERS

ACI is accepting the submission of papers for conventions, committees, chapters, and subsidiaries. Detailed descriptions of submission requirements and policies can be found at www.concrete.org. ACI's website also contains a detailed list of the date(s), sponsor(s), and location(s) of events calling for papers.

Guidelines for submitting technical papers for review to either the *ACI Structural Journal* or the *ACI Materials Journal* can be found at ACI's website.